energies

MDPI

Article

Comparison of Electromagnetic Characteristics of Single-Phase Induction Motor between Balanced and Unbalanced Operation under Different Loads

Dae Yong Um and Gwan Soo Park *

Department of Electrical and Computer Engineering, Pusan National University, Busan 46241, Korea; daeyongum@pusan.ac.kr

* Correspondence: gspark@pusan.ac.kr; Tel.: +82-51-510-2788

Abstract: This paper varies load conditions in a single-phase induction motor and deals with consequent effects on the electromagnetic characteristics in terms of a balanced and unbalanced operation. Based on a balanced-load condition, the magnetic field, electromagnetic losses, magnetic torque are quantified by the time-stepping finite element method at six different loads. The spatial distribution of the air-gap magnetic field are investigated to characterize the existence between the load variation and unbalanced operation. The components of electromagnetic losses are analyzed in terms of main parameters degrading the operating efficiency according to the load variation. The result can show the importance of building the magnetic balance for a high performance, and the design guideline for SPIMs running at multiple operating points is discussed.

Keywords: backward rotating magnetic field; electromagnetic losses; finite element method; magnetic balance; single-phase induction motor

Citation: Um, D.Y.; Park, G.S. Comparison of Electromagnetic Characteristics of Single-Phase Induction Motor between Balanced and Unbalanced Operation under Different Loads. *Energies* **2021**, *14*, 919. https://doi.org/10.3390/en14040919

Academic Editor: José A.F.O. Correia

Received: 21 December 2020

Accepted: 4 February 2021

Published: 9 February 2021

1. Introduction

Single-phase induction motors (SPIMs) are widely used in various industrial and household applications where a single-phase source is solely available. Two-pole SPIMs are constructed by main and auxiliary windings, which are in space quadrature. In addition, impedance of both windings is adjusted by geometrical changes or additional capacitors to split into two-phase sources. Even though decreasing prices of inverter-fed drive have spread to operate two-phase or three-phase motors electronically, but SPIMs still have strong merits for its simplicity and maintenance [1–4].

SPIMs are generally classified into split-phase, capacitor-start, capacitor-run types. Split-phase SPIMs have been evaluated to poor starting and running performance, which lead to limit their application. The problem can be solved by connecting the capacitor in series into the auxiliary winding. The capacitor has an essential role to adjust equivalent impedance of the auxiliary winding, thus the magnitude and phase of current into windings can be split properly to avoid magnetically unbalanced condition.

Many authors have conducted researches on optimal design, numerical, and analytical analysis of SPIMs. They developed improved SPIMs by geometrical changes [5–8], and adapting control strategies of an electronic circuit [9–11]. In addition, some studies [12] have suggested operating scheme of SPIMs using three-phase windings where the two capacitors are used to operate from single-phase supply. The additional winding and capacitor lead to a higher degree of freedom to make the operating performance approximately same as three-phase induction motor. Unfortunately, all SPIMs have an inherent problem, which comes from a highly unbalanced poly-phase magnetic system, so that magnetic unbalance occurs almost all operating points except for the specific operating point. Many papers successfully have concluded their studies, but there are relatively a lack of quantifying the effect of unbalanced operation on electromagnetic quantities such as magnetic field, losses, force and

torque, and design approach considering a wide range of loads. Generally, the magnetically unbalanced operation induces backward rotating magnetic field (RMF), which lead to a negative torque with respect to a rotating direction of the rotor. Furthermore, elliptical stator magnetomotive force (MMF) can distort the current distribution of bar current, a temporal waveform and spatial distribution of the magnetic field. This unbalanced distribution can increase the stator copper loss, the core loss in both stator and rotor core and eddy current loss in rotor bars, which deteriorate the operating efficiency. More severe problems are high torque ripple and unbalanced magnetic force, leading to the vibration, acoustic noise and poorer performance of applications.

Many applications recently have demanded more than a single operating point, thus many problems caused by the unbalanced operation are inevitable in SPIMs, which are running at multiple operating point. Besides, the loading condition can be affected by the integrated system such as air conditioning applications. For instance, the loading condition of air-conditioning compressor can be varied due to the change of flow rate of the air [13]. Considering a SPIM applicable to various application, a more quantitative investigation on the operating characteristics of SPIMs running under unbalanced operation is needed.

The author previously studied the design approach for the magnetically balanced operation by making the circular stator MMF for the target load condition [14]. Based on the published model, the initial model is re-designed for a balanced-load condition, and adverse effects on the model are analyzed when the load torque deviates from the balanced operation. The spatial distribution of air-gap magnetic flux density and rotor bar currents are computed by time-stepping finite element analysis [15–17]. The electromagnetic losses are decomposed into copper loss in stator windings, eddy current loss in rotor bars, core loss, and negative torque caused by the harmonic rotating magnetic field. The loss components are normalized with respect to total losses, thus the major loss components which deteriorate the operating efficiency are illustrated. Finally, possible schemes are discussed and suggest the design guidelines to keep the superiority of balanced operation when SPIMs are designed to run for multiple loads.

2. Computation of Electromagnetic Characteristics

In this section, calculation of electromagnetic quantities is described to illustrate the effect of unbalanced operation. The computation procedures are shown based on the finite element analysis and characterization of unbalanced operation prior to the calculation. We select a commercial capacitor-run SPIM, and the size and specification of the motor are listed in Table 1.

Table 1. The parameters of the capacitor-run SPIM model.

Parameter	Value	Parameter	Value
Rated power	2600 W	Stator outer diameter	139 mm
Rated voltage	230 Vrms	Number of rotor slots	34
Frequency	60 Hz	Rotor outer diameter	71 mm
Number of poles	2	Stack length	105 mm
Number of stator slots	24	Running capacitor	45 μF
Number of turns in the main winding	162	Number of turns in the auxiliary winding	160

The distribution of magnetic field can be calculated by given winding configurations, currents and the geometry of the stator and rotor cores, thus stator MMF is determined by theses parameters. In Figure 1, the stator MMF primarily acts to magnetize the machine and then the induced current in every rotor bar creates a reaction field, which is energized by the rotor MMF. Then, the total magnetizing MMF can be written as the sum of stator and rotor MMF and this creates the air-gap magnetic field. The phase of magnetizing MMF is about 90 degrees ahead of that of rotor MMF, which follows the faraday's law and δ is a phase shift due to the leakage inductance of rotor core. Subtracting magnetizing and

rotor MMF can derive the stator MMF, which is ϕ_m degrees ahead of magnetizing MMF according to the loading condition.

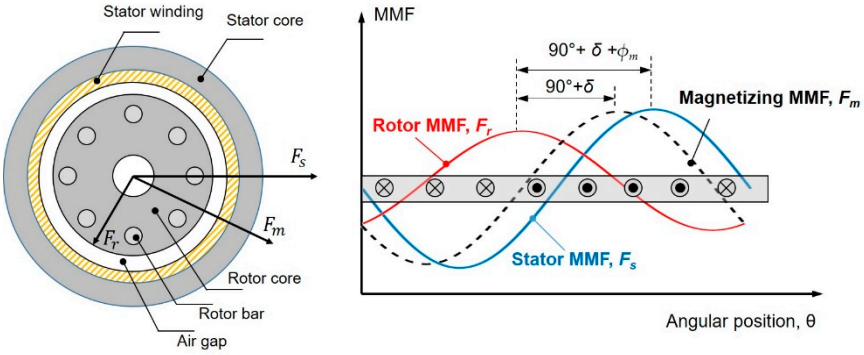

Figure 1. Schematic diagram for the description of MMF components in an induction machine.

Assuming the infinite permeability of stator and rotor core and uniform air-gap length, the air-gap magnetic flux density B_g is

$$B_g(\theta,t) = F_m(\theta,t)\cdot\Lambda(\theta) = [F_s(\theta,t) + F_r(\theta,t)]\cdot\Lambda(\theta) \quad (1)$$

$$\Lambda(\theta) = \Lambda_0 + \sum_k (\Lambda_{ks}\cos(kq_s\theta) + \Lambda_{kr}\cos(kq_r\theta)) \quad (2)$$

where q_s and q_r are the number of stator and rotor slot, respectively, Λ_0 is constant term and Λ_{ks} and Λ_{kr} are the k-th spatial harmonic component of a permeance due to stator and rotor slot, respectively. The stator and rotor MMF in (1) include the slotting effect of stator and rotor core as well as the current distribution in windings and rotor bars. The slot harmonics in (2) is dependent on the load condition.

The stator MMF generated by sinusoidally distributed main and auxiliary windings at arbitrary phase angle α and β can be represented as follows:

$$\begin{aligned} F_s(\theta,t) = {} & \tfrac{N_m I_m}{2}\cos(2\pi f_s t + \alpha - p\theta) + \tfrac{N_a I_a}{2}\cos\left(2\pi f_s t + \beta - p\left(\theta + \tfrac{\pi}{2}\right)\right) \\ & + \tfrac{N_m I_m}{2}\cos(2\pi f_s t + \alpha + p\theta) + \tfrac{N_a I_a}{2}\cos\left(2\pi f_s t + \beta + p\left(\theta + \tfrac{\pi}{2}\right)\right) \end{aligned} \quad (3)$$

where N_m and N_a are the total number of turns in main and auxiliary winding respectively, I is the peak value of the winding current and f_s is the supply frequency. Spatial and temporal distribution of the stator MMF is compared between two specific load conditions, as described in Figure 2. In balanced-load condition, the stator MMF with respect to the fundamental frequency rotates with the same magnitude at the fundamental frequency, but the fluctuation increases as the operation deviates from balanced condition.

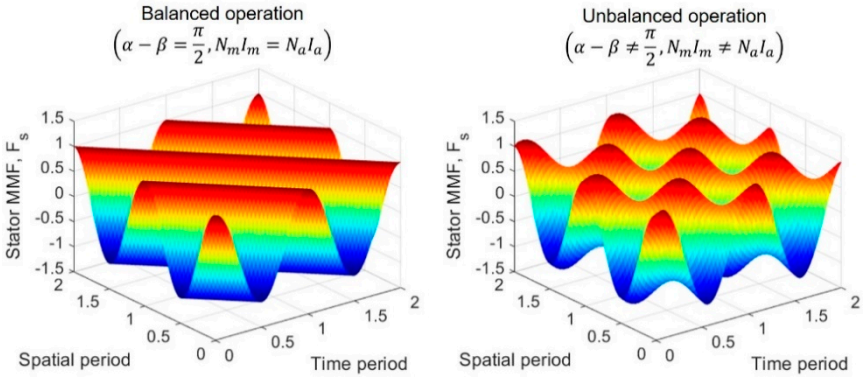

Figure 2. Spatial and temporal distribution of stator MMF at the balanced and unbalanced operation.

Unlike the stator MMF, the trajectory of magnetizing MMF is rather a circular shape, referring to some researches [3]. This is because the reaction field created by rotor MMF, thus the resultant field MMF can be simplified as the term of only forward rotating field, as written as:

$$F_m(\theta, t) = F_s(\theta, t) + F_r(\theta, t) = F\cos(2\pi f_s t - \phi_m - p\theta) \tag{4}$$

Equation (4) indicates that the rotor MMF also have the term of backward RMF caused by the distribution of the stator MMF. Since the rotor MMF are created by bar currents, the effect of the unbalance condition can be characterized by analyzing the distribution of rotor bar currents using finite element analysis.

For quantitative separation of loss components using finite element analysis, stator copper loss, rotor bar loss, core-loss, and loss caused by backward RMF are calculated separately. The stator copper loss is expressed as follows using resistance calculated by reflecting the current and end winding structure of each phase.

$$P_{copper} = \frac{1}{T}\int_0^T \left(i_m(t)^2 R_m + i_a(t)^2 R_a\right) dt \tag{5}$$

where T is the time period, R_m, R_a are the main and auxiliary winding resistance including the end-winding, and i_m, i_a are the instantaneous main and auxiliary winding currents, respectively.

The rotor bar loss is the sum of the eddy current loss throughout rotor bar calculated using the calculated magnetic vector potential A_b.

$$P_{bar} = \frac{1}{T}\sum_{v=1}^{N_b}\int_0^T \int_{bar} \frac{1}{\sigma}|j_{bv}(t)|^2 dv dt = \frac{1}{T}\sum_{v=1}^{N_b}\int_0^T \int_{bar} \sigma\left|\frac{dA_{bv}}{dt}\right|^2 dv dt \tag{6}$$

Core-loss can be estimated by the steinmetz equation and high order harmonics should be considered to reflect the distortion of magnetic field and current waveform because ignorance of harmonic components can lead to large error of the estimation [18]. Equation (7) shows that the core-loss contains the series expression of n times harmonics obtained by using Fourier transform of the magnetic flux density waveform in each element of stator and rotor core:

$$P_{core} = \int_{core}\sum_n \left[c_h(nf_s)|B_n|^2 + c_c(nf_s)^2|B_n|^2 + c_e(nf_s)^{1.5}|B_n|^{1.5}\right] dv \tag{7}$$

where c_h, c_c and c_e are the hysteresis, classical eddy current, excess loss coefficients, respectively. These coefficients can be obtained by curve fitting from manufacturer's data and various frequency data are needed to calculate harmonic core-loss from exact interpolation with respect to wide frequency range. In this study, we set the constant core-loss coefficients measured at 60 Hz at all harmonic components. This is because the stator and rotor core are typically the silicon steel laminations, thus their thickness is much smaller than the skin depth at 60 Hz fundamental frequency and its space harmonic. However, an induction motor fed by a pulsewidth modulated (PWM) inverter, which have much higher fundamental frequency and carrier frequency needs variable core-loss coefficients with respect to the harmonic frequency.

The electromagnetic torque can be calculated by using the distribution of radial and tangential components B_r, B_θ of air-gap magnetic flux density,

$$T_e(t) = \oint_{airgap} \vec{r} \times \vec{f} \cdot d\vec{S} = \oint_{airgap} r_g\left(\frac{1}{\mu_0} B_r B_\theta\right) \cdot dS \tag{8}$$

where r_g represents the radius of the air gap, f is surface force density, which can be calculated by using Maxwell stress tensor method. In Equation (8), the radial component of magnetic field describes the total magnetizing MMF. In addition, the tangential component of magnetic field is discontinuous on the boundary of cores, which corresponds to the

equivalent surface current on the boundary. Assuming the infinite permeability of core, and stator winding and rotor bar current as a surface current sheet, the tangential component of magnetic field can be equivalent to the distribution of stator or rotor MMF. Consequently, torque waveform follows the shape of stator MMF and the pulsating torque can be very significant under unbalanced operation.

In SPIMs, the input power is the sum of the mechanical power with respect to the positive and negative torque, stator copper loss, rotor bar loss and core-loss, as follows:

$$P_i = T_f \cdot \omega_m + T_b \cdot \omega_m + P_{copper} + P_{bar} + P_{core} \tag{9}$$

Since core-loss is not included during the simulation and obtained separately in the post-processing, the relationship between input power and output power can be written as (10). In the right hand side of Equation (10), the first term indicates the mechanical output and the last term is the loss caused by the backward RMF. Then, using known values obtained by FEM and combining (9) into (10) can represent the negative torque caused by backward magnetic field in (11).

$$P_i^{FEM} = P_o^{FEM} + P_{copper}^{FEM} + P_{bar}^{FEM} = \left(T_f - T_b\right)\omega_m + P_{copper}^{FEM} + P_{bar}^{FEM} + 2T_b\omega_m \tag{10}$$

$$T_b^{FEM} = \frac{1}{2}\frac{P_i^{FEM} - P_o^{FEM} - P_{copper}^{FEM} - P_{bar}^{FEM}}{\omega_m} \tag{11}$$

The efficiency can be obtained by substituting (10) into (9), which is represented as

$$\eta = \frac{P_o}{P_i} = \frac{P_o^{FEM}}{P_i^{FEM} + P_{core}^{FEM}} \tag{12}$$

The stator winding currents, phase difference and efficiency are calculated, and the results obtained at 60% and 100% loads are compared with measured results in Table 2.

Table 2. Comparison of the calculated and measured results at 60% and 100% loading condition.

Parameter	100% Load		60% Load	
	Calculated	Measured	Calculated	Measured
Total current (A)	13.258	13.410	8.200	8.302
Main winding current (A)	11.176	11.045	7.422	7.341
Auxiliary winding current (A)	5.367	5.443	5.684	5.747
Phase difference (deg)	79.450	79.588	103.890	102.464
Power factor	0.975	0.979	0.954	0.961
Efficiency (%)	87.332	87.290	86.563	85.720

Since the calculation at two different loads estimates the operating performance well, compared with the measured value. In Section 3, the initial model is redesigned for the balanced-load condition at the rated load, referring to our previously published paper [14]. The running capacitor and the number of turns in two windings are changed compared with the initial model.

3. Analysis of the Effect of Unbalanced Operation

The FE model is constructed and time-stepping fields are solved by a commercial FEM software, Ansys-Maxwell 2D-transient solver. In this paper, the simulation covers the steady-state quantities under different loads (55%, 70%, 85%, 100%, 115%, and 130% load). The varied parameters for the redesigned model is shown in Table 3.

Table 3. The modified parameters tuning for the balanced-load condition at the rated load.

Parameter	Initial	Redesigned
Running capacitor (μF)	45	90.7
Number of turns in main winding, N_m	162	164
Number of turns in main winding, N_a	160	130
Turns ratio, N_a/N_m	0.988	0.793

The calculated current and phase are illustrated in Table 4. For the balanced-load condition, the current ratio defined in Table 4 should be equal to the turns ratio in Table 3. Additionally, the phase difference between main and auxiliary current should be 90 degrees, thus the redesigned model is properly redesigned for the rated load. The efficiency of the SPIM becomes maximum and decreases significantly at the lighter load.

Table 4. The comparison of operating performance at different loads.

Parameter	55%	70%	85%	100%	115%	130%
Input current (A)	8.181	9.774	11.463	13.218	15.050	16.961
Main winding current, I_m (A)	5.501	5.728	6.405	7.978	9.712	11.732
Auxiliary winding current, I_a (A)	11.135	10.906	10.698	10.488	10.268	10.032
Current ratio, I_m/I_a	0.494	0.525	0.599	0.761	0.946	1.169
Phase difference (deg)	135.676	116.828	100.909	89.634	82.283	77.725
Power factor	0.928	0.951	0.967	0.979	0.987	0.994
Output power (W)	1473	1867	2258	2644	3025	3401
Efficiency (%)	82.096	85.259	86.843	87.430	87.303	86.592

Figure 3 represents the spatial waveform of the stator MMF, which is obtained by the calculated current waveform. The magnitude and phase of the main and auxiliary winding current in Table 4 are substituted in (3), and the fluctuation of stator MMF increases significantly as the operating load is away from the balanced-load condition. This unbalanced RMF can affect the distribution of rotor bar currents, and the consequent winding and rotor bar losses.

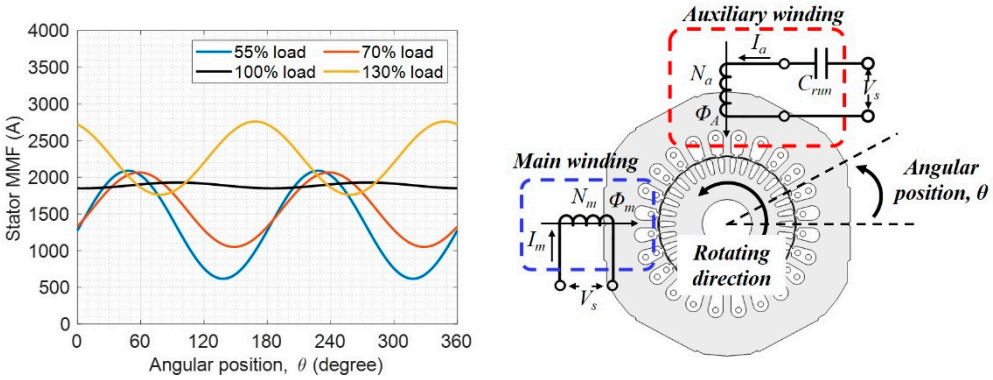

Figure 3. Stator MMF waveform using calculated current in windings under different loads.

Figure 4 shows the air-gap magnetic flux density and the rotating magnetic field obtained by using 2-D fourier transform of spatial and temporal magnetic field waveform. Each value of rotating field is the peak value of the fundamental component of the magnetic flux density at each load. In Figure 4a, the magnetic flux density is presented when the main winding current is maximum, and it can be seen that the phase of the magnetic flux density changes due to the phase difference between the main and auxiliary winding current. Referring to the dotted circle in Figure 4, it can be seen that the rotating magnetic field is rather circular, which does not match that of the stator MMF. This is because the

rotor MMF can alleviate the unbalance so that the air-gap magnetic field is not sensitive to the unbalanced condition.

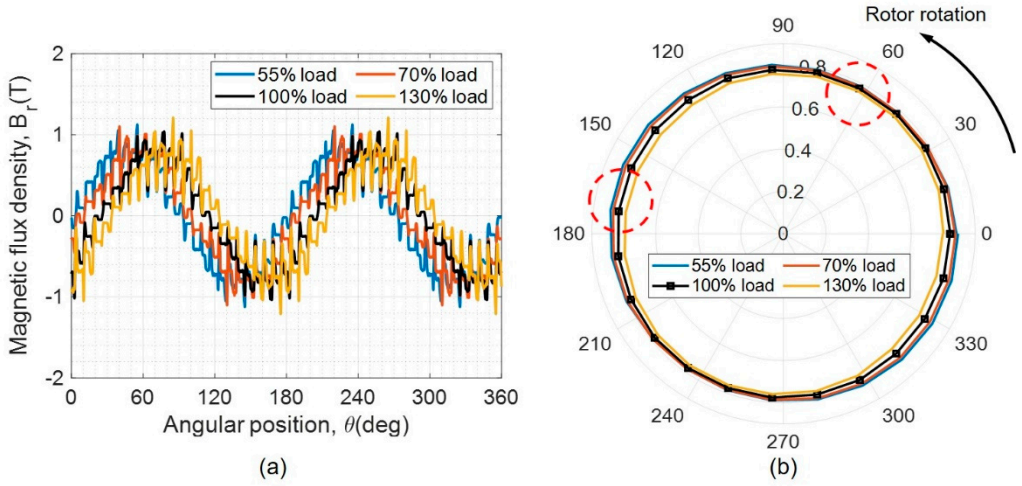

Figure 4. (**a**) The air-gap magnetic flux density and (**b**) the trajectory of the rotating magnetic field.

As shown in Table 5, electromagnetic losses are calculated at the different loads. The stator copper loss and rotor bar loss tend to decrease monotonically when the value of load decreases. However, the decrease rate steadily becomes small and the stator copper loss at 55% load increases despite of the lighter load. The core-loss is insignificant to the change of loads since the air gap magnetic field is rarely affected by the unbalanced condition. The contribution of negative torque is notable, but the absolute value of the change rate with respect to the different loads is not quite distinct.

Table 5. The comparison of electromagnetic losses at different loads.

Parameter	55%	70%	85%	100%	115%	130%
Stator copper loss (W)	147.864	146.343	155.155	174.945	207.315	254.511
Rotor bar loss (W)	51.730	58.275	69.850	87.339	112.460	147.102
Core-loss (W)	59.252	57.876	57.176	56.988	57.315	58.019
Loss caused by negative magnetic field (W)	62.508	60.382	60.096	61.218	63.526	67.888

The losses described in Table 5 are difficult for the fair comparison due to its different input power, so that losses are normalized by the input power at each load. As illustrated in Figure 5, the portion of stator copper loss becomes minimum when the SPIM is running at the balanced-load condition. This is because the current is evenly distributed between the main and auxiliary winding, which is the criteria for the balanced operation of SPIMs. In general, the eddy current loss in the rotor bar increases when the heavier load is applied and the rotating speed of rotor is slower. However, the portion of rotor bar loss is almost equal or increases below balanced-load condition. The reduction of rotor bar loss can make the operating efficiency higher, which is the merit of the balanced operation. In case of the core-loss, its portion steadily decreases because the absolute value of the core-loss is not really affected by both change of loads and the unbalanced condition. The backward RMF makes the braking torque and this torque is almost constant despite of the lighter loading condition. Thus, the loss can be approximate to the constant at operating loads so that the portion of the loss increases at the lighter load.

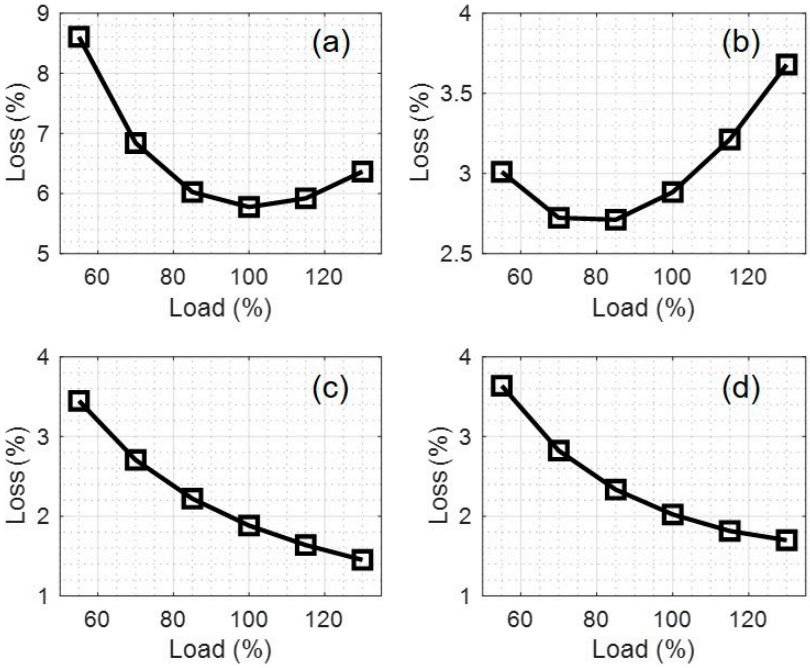

Figure 5. Loss components normalized in percentage under different loads. (**a**) Stator copper loss (**b**) Rotor bar loss (**c**) Core-loss (**d**) Loss caused by backward magnetic field.

Figure 6 shows the torque waveform calculated at the different loads. As the load deviates from the balanced condition, the torque ripple largely increases. The waveform in Figure 6 is similar to that of the stator MMF in Figure 3. This is because the calculation of the torque contains the tangential component of magnetic field in (8), which follows the waveform of the stator MMF. Especially, the torque ripple increases more significantly at the lighter loads, which is the same trend of the efficiency variation at the lighter loads. If SPIM operates at multiple operating loads except for the balanced-load condition, optimal design focusing on the target load can deteriorate the operating performance at other operating points, especially at the lighter load. Therefore, the selection of the proper load is required for the application using multiple operating loads, and this will be discussed in Section 4.

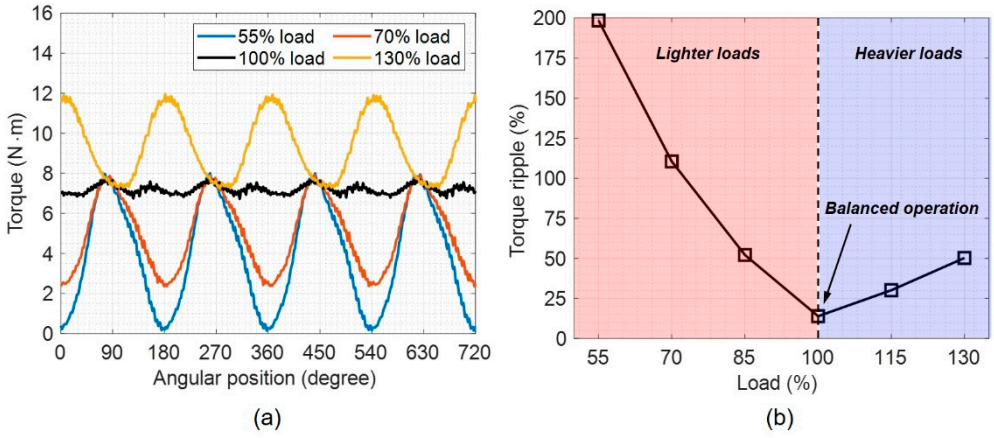

Figure 6. (**a**) The torque waveform and (**b**) torque ripple at the different loads.

4. Discussion

The result indicates how the unbalanced operation affects the electromagnetic quantities such as the air-gap magnetic field, the subsequent losses, torque. The loss caused by the backward RMF occupies a large portion of total losses, but the absolute value is

not sensitive to the change of loads. The torque ripple dramatically increases under unbalanced operation. The air-gap magnetic field is rather circular, but the stator and rotor MMF can be still distorted because of uneven distribution of currents. The Lorentz force on stator windings and rotor bars can be applied and the distribution of force will follow the distribution of each current. Since the force is proportional to the current flowing into the rotor bar, the uneven distribution of current can lead to magnify the force on the rotor bar. The locally concentrated force will make the vibration and acoustic issue. Thus, the design of SPIMs can face the bottleneck unless the SPIM is primarily designed to run at the balanced-load condition and the further research dealing with the electromagnetic force and its structural effects is necessary. In Section 3, we developed the redesigned model and the model shows the improvement of the performance. However, the disadvantages of making balanced-load condition at the rated load is that the operating characteristics drastically deteriorate compared with the balanced operation. Therefore, it is necessary to find a suitable design target point when SPIM is not used at the fixed operating point. Additionally, redesigned model is dealt to compare with the models designed for the different loads. In the same method, the capacitor and the number of turns in windings are changed and their values are shown in Table 6.

Table 6. The parameters tuning the balanced condition at 100% and 75% loads.

Parameter	Initial	Redesigned at 100% Load	Redesigned at 75% Load
Running capacitor (μF)	45	90.7	70
Number of turns in main winding, N_m	162	164	177
Number of turns in main winding, N_a	160	130	134
Turns ratio, N_a/N_m	0.988	0.793	0.757

Figure 7 illustrates the efficiency and torque ripple of each model at different load. Compared to the model designed for 100% load, the model designed for 75% load shows wider operating efficiency characteristics for both the rated and lighter loads. In particular, the model designed for the 100% load shows the lower efficiency than that of the original model at the lighter load. On the other hand, the model designed for 75% load not only exhibits high overall characteristics compared to the initial model, but also shows higher efficiency characteristics than the designed model for the 100% load. Torque ripple has the similar tendency to the efficiency. However, the torque ripple is minimum at the balanced condition and increases rapidly as it is away from the balance, thus the efficiency and torque characteristics must be considered mutually.

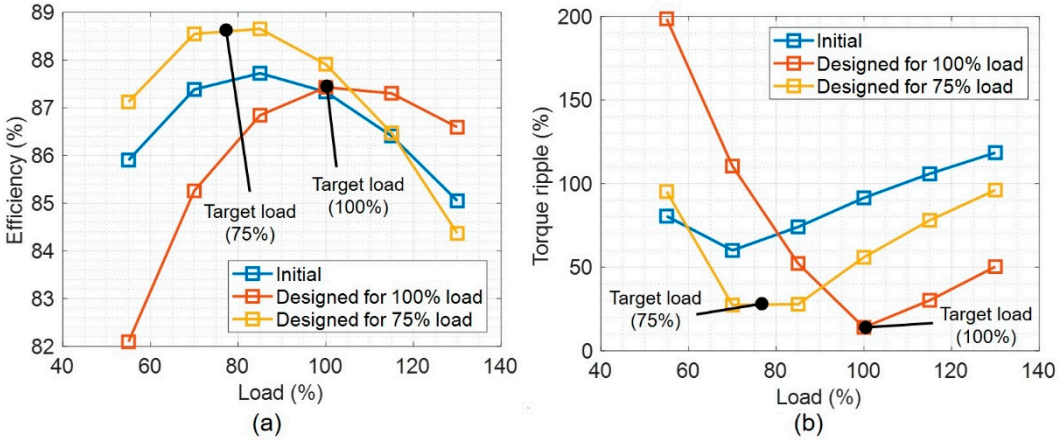

Figure 7. (**a**) The efficiency and (**b**) torque ripple of initial and two designed model at different loads.

Further, typical SPIMs run with a capacitor to generate the rotating magnetic field, and the frequency response of SPIM has a unique operating point for the magnetically balanced condition. The idea is to adjust the frequency response of SPIM to the desired loading condition, or increase the order of the frequency response to make multiple balanced conditions. The former usually can be solved by utilizing the various frequency inverter to adjust the supply frequency [9–11]. The latter can be achieved by the pole changing method or adding multiple capacitor with poly-phase windings [5–8,12].

5. Conclusions

In this paper, the effects of unbalanced operation on the performance of SPIM are investigated at the different loads. The currents, losses and torque waveform are calculated by using the finite-element analysis. The characteristics of SPIM under different loads and unbalanced operation is summarized below:

- The stator MMF reflects the unbalanced operation and affects the rotor MMF.
- The unbalanced stator winding, and rotor bar currents increases the loss and degrade the efficiency.
- The loss caused by backward magnetic field has large portion and its portion is larger at the lighter loads.
- The pulsating torque deteriorates as the load deviates from the balanced condition and significantly increases at the lighter loads.
- Proper selection of the target load should be considered to operate the SPIM at various load condition.
- The electromagnetic force on the stator winding and rotor bars should be considered for the vibration and structural analysis, and the effect of unbalanced condition on these force will be the future research.

That is, the electromagnetic quantities deteriorate significantly when SPIM run at the unbalanced condition, showing the importance of equilibrium design. Finally, the result provides the importance to operate SPIMs at the balanced condition so that the loading condition and load variations of an application should be considered in advance when we design SPIMs.

Author Contributions: Conceptualization, D.Y.U. and G.S.P.; software, D.Y.U.; validation, D.Y.U. writing, D.Y.U. and G.S.P. All authors have read and agreed to the published version of the manuscript.

Funding: This research received no external funding.

Conflicts of Interest: The authors declare no conflict of interest.

References

1. Liu, Y.; Vittal, V.; Undrill, J.; Eto, J.H. Transient model of air-conditioner compressor single phase induction motor. *IEEE Trans. Power Syst.* **2013**, *28*, 4528–4536. [CrossRef]
2. Haddad Kalluf, F.J.; Tutelea, L.N.; Boldea, I.; Espindola, A. 2/4-POLE Split-Phase Capacitor Motor for Small Compressors: A Comprehensive Motor Characterization. *IEEE Trans. Ind. Appl.* **2014**, *50*, 356–363. [CrossRef]
3. Rasmussen, C.B.; Miller, T. Revolving-field polygon technique for performance prediction of single-phase induction motors. *IEEE Trans. Ind. Appl.* **2003**, *39*, 1300–1306. [CrossRef]
4. Umans, S.D. Steady-state, lumped-parameter model for capacitor-run, single-phase induction motors. *IEEE Trans. Ind. Appl.* **2002**, *32*, 169–179. [CrossRef]
5. Nam, H.; Jung, S.; Kang, G.; Hong, J.; Jung, T. Design of pole change single-phase induction motor for household appliances. *IEEE Trans. Ind. Appl.* **2004**, *40*, 780–788. [CrossRef]
6. Ojaghi, M.; Daliri, S. Analytic model for performance study and computer-aided design of single-phase shaded-pole induction motors. *IEEE Trans. Energy Convers.* **2017**, *32*, 649–657. [CrossRef]
7. Mera, R.; Campeanu, R. Optimal performance of capacitor-run single phase induction motor. In Proceedings of the 2012 13th International Conference on Optimization of Electrical and Electronic Equipment (OPTIM), Brasov, Romania, 24–26 May 2012; Institute of Electrical and Electronics Engineers (IEEE): Piscataway, NJ, USA, 2012; pp. 718–723.
8. Tekgun, B.; Sozer, Y.; Tsukerman, I. Modeling and parameter estimation of split-single phase induction motors. *IEEE Trans. Ind. Appl.* **2015**, *52*, 1431–1440. [CrossRef]

9. Lettenmaier, T.M.; Novotny, D.W.; Lipo, T.A. Single phase induction motor with an electronically controlled capacitor. *IEEE Trans. Ind. Appl.* **2003**, *27*, 38–43. [CrossRef]
10. Mademlis, C.; Kioskeridis, I.; Theodoulidis, T. Optimization of single-phase induction motors—Part I: Maximum energy efficiency control. *IEEE Trans. Energy Convers.* **2005**, *20*, 187–195. [CrossRef]
11. Blaabjerg, F.; Jungeanu, F.; Skaug, K.; Tonnes, M.; Lungeanu, F. Two-phase induction motor drives. *IEEE Ind. Appl. Mag.* **2004**, *10*, 24–32. [CrossRef]
12. Xiuhe, W.; Hui, Z.; Yubo, Y.; Xiaolei, M. Study of a novel energy efficient single-phase induction motor with three series-connected windings and two capacitors. *IEEE Trans. Energy Convers.* **2010**, *25*, 433–440. [CrossRef]
13. Kini, P.G.; Bansal, R.C. Effect of Voltage and Load Variations on Efficiencies of a Motor-Pump System. *IEEE Trans. Energy Convers.* **2009**, *25*, 287–292. [CrossRef]
14. Um, D.Y.; Park, G.S. Determination scheme of stator parameters for making rotating fields circular in a single-phase induction motor. *IEEE Trans. Magn.* **2020**, *56*, 1–5. [CrossRef]
15. De Gersem, H.; Hameyer, K. Air-gap flux splitting for the time-harmonic finite-element simulation of single-phase induction machines. *IEEE Trans. Magn.* **2002**, *38*, 1221–1224. [CrossRef]
16. Wang, X.; Zhu, C.; Zhang, R.; Tang, R.; Song-Yop, H. Performance analysis of single-phase induction motor based on voltage source complex finite-element analysis. *IEEE Trans. Magn.* **2006**, *42*, 587–590. [CrossRef]
17. Sorrentino, E.; Fernández, S. Comparison of six steady-state models for single-phase induction motors. *IET Electr. Power Appl.* **2011**, *5*, 611. [CrossRef]
18. Yazdani-Asrami, M.; Mirzaie, M.; Akmal, A.A.S. No-load loss calculation of distribution transformers supplied by nonsinusoidal voltage using three-dimensional finite element analysis. *Energy* **2013**, *50*, 205–219. [CrossRef]